Neuropsychiatric Disease and Treatment

Dovepress
Taylor & Francis Group

Open Access Full Text Article

ORIGINAL RESEARCH

Multimodal Magnetic Resonance Findings in Parkinson's Disease With "Antecedent Essential Tremor": A Case Series of a Large Kindred

Yu Kong[1,*], Lei Yao[2,*], Xiangyu Xiao[2,3], Anqiang Chen[1], Kexin Wang[1], Huan Yan[4], Ran Sun[4], Ruihan Liu[5,6,*], Qingxia Kong[4,*]

[1]Medical Imaging Department, Affiliated Hospital of Jining Medical University, Jining, Shandong, 272000, People's Republic of China; [2]Clinical Medical College, Jining Medical University, Jining, Shandong, 272000, People's Republic of China; [3]Cheeloo College of Medicine, Shandong University, Jinan, Shandong, 250012, People's Republic of China; [4]Department of Neurology, Affiliated Hospital of Jining Medical University, Jining, Shandong, 272029, People's Republic of China; [5]Department of Pediatrics, Affiliated Hospital of Jining Medical University, Jining, Shandong, 272029, People's Republic of China; [6]Postdoctoral Mobile Station of Shandong University of Traditional Chinese Medicine, Jinan, Shandong, 250012, People's Republic of China

*These authors contributed equally to this work

Correspondence: Qingxia Kong, Department of Neurology, Affiliated Hospital of Jining Medical University, 89 Guhuai Road, Jining, Shandong, 272000, People's Republic of China, Email kxdqy8@sohu.com; Ruihan Liu, Department of Pediatrics, Affiliated Hospital of Jining Medical University, 89 Guhuai Road, Jining, Shandong, 272000, People's Republic of China, Email ruihanliu1987@163.com

Background: The clinical pictures of essential tremor (ET) and Parkinson's disease (PD) are often quite mimic at the early stage, and longstanding ET may ultimately develop to PD, that is, PD with "antecedent ET". Early diagnosis and differentiation of the two are essential for predicting disease progression and formulating individualized treatment plans. However, current approaches remain challenging. This study aimed at determining the morphological, microstructural and iron-related changes in these patients' brains using multimodal magnetic resonance imaging (MRI).

Methods: We reviewed a kindred with ET and PD with "antecedent ET" recruited at our hospital in May 2023. The clinical characteristics, genetic testing and multimodal MRI data of 16 family members were collected. Multimodal MRI analysis included structural MRI, diffusion tensor imaging (DTI) and tractography, and quantitative susceptibility mapping (QSM).

Results: Two second-generation family members diagnosed PD had ET history before PD performance appeared, five third-generation family members were diagnosed with ET. Fifteen of the 16 cases had missense mutation in the EIF4G1 gene. Temporal and spatial features of morphology and iron deposition in different brain regions were heterogeneous. DTI showed that the cerebello-thalamo-motor cortical network was involved in both ET and PD cases, and the additional nigrostriatal-thalamo-motor cortical network was involved in PD cases.

Conclusion: The combination of morphometric imaging, DTI and QSM could be used as an imaging biomarker for ET and PD diagnosis and could be an effective tool for longitudinal monitoring of disease progression and transformation.

Keywords: magnetic resonance imaging, quantitative susceptibility mapping, diffusion tensor imaging, Parkinson's disease, essential tremor, eukaryotic translation initiation factor 4 gamma 1

Introduction

Parkinson's disease (PD) and essential tremor (ET) are prevalent chronic movement disorders in the general population. ET is the most common tremor disorder, with bilateral tremors occurring during actions.[1] PD is a prevalent neurodegenerative disease. Tremors in patients with PD commonly occur at rest, present unilaterally, and progress to both sides of the body. PD encompasses additional symptoms, like bradykinesia, rigidity, and gait or balance issues.[2–4] ET and PD are difficult to distinguish because they have the same clinical symptoms, particularly in disease early stages. In addition, longstanding clinical research has demonstrated that patients with prolonged ET may eventually develop other neurological conditions, like dystonia or PD, those who later exhibit a PD phenotype are described as having PD with

Received: 30 September 2024
Accepted: 13 January 2025
Published: 22 January 2025

"antecedent ET".[5] However, whether ET has a potential risk of developing to PD remains controversial. Therefore, in view of the fact that the clinical pictures of ET and PD are often quite similar and that these two diseases can transform into each other, current methods to early diagnosis and individualized therapy remain challenging.[6]

Neuroimaging techniques have been widely applied to identify structural and functional brain abnormalities across different diseases. Dopamine transporter single-photon emission computed tomography (SPECT) / positron emission tomography (PET) can effectively differentiate degenerative parkinsonism from other conditions, such as ETs, with high sensitivity and specificity.[7,8] However, its application has been limited owing to the difficulty in preparing imaging agents and radiation exposure during examination. Therefore, magnetic resonance imaging (MRI) was introduced to reveal the brain imaging features of PD or ET.[7,9,10] These studies mostly compared the brain images of patients with PD or ET with those of normal controls. Limited neuroimaging studies have focused on the distinctions and associations between these two diseases. No specific imaging features were observed on structural MRI between these two diseases in previous studies. Diffusion tensor imaging (DTI) and tractography could be applied to explore features of ET and PD as they are able to show altered white matter (WM) microstructural integrity of brain and delineation of specific fiber pathways. The pathogenesis of PD is still unclear, mainly involving genetic, environmental and neurobiological levels, so the treatment interventions are diverse.[11–15] Some researches suggested that iron deposition may be a potential pathogenic mechanism.[16] Therefore, iron may be a therapeutic target for PD, and the distribution of iron in different brain regions may affect the formulation of therapeutic intervention programs and therapeutic effects.[17] It is necessary to precisely localize the brain region of iron deposition and accurately quantify the iron content in the brain region. A previous study used quantitative susceptibility mapping (QSM) to assess iron deposition in different brain regions of PD patients in vivo and found spatial-temporal variations in iron distribution in PD brains, particularly in deep gray matter (GM) structures.[18,19] The application of QSM is of great significance for early precise diagnosis and monitoring of disease progression.[20] However, there are few reports on the application of QSM to quantitative ET analysis.[21] To date, there has been a lack of stable neuroimaging biomarkers for identifying and differentiating ET from PD at an individual level.

Early diagnosis is crucial to predict the course of these diseases. In this study, we performed multimodal MRI in a kindred with ET and PD with "antecedent ET" and attempted to identify neuroimaging biomarkers for early differential diagnosis of PD and ET using a longitudinal study. Thus, establishing an appropriate medical follow-up mechanism based on neuroimaging may assist in the clinical development of individualized treatment plans and delay disease progression.

Methods

Clinical Characteristics

The family was recruited in May 2023 and underwent clinical and genetic evaluations at the Affiliated Hospital of Jining Medical University. Clinical data and data related to various examinations were collected by specialist neurologists blinded to the participants' histories. PD diagnosis followed the United Kingdom Parkinson's Disease Society Brain Bank clinical diagnostic criteria with severity evaluated via the Movement Disorder Society-sponsored revision of the United PD Rating Scale (UPDRS) Part III. The diagnostic criteria for ET were established according to the classification by the International Parkinson and Movement Disorder Society's Task Force on Tremors. Cognitive impairment was assessed with the Chinese version of the Mini-Mental State Examination (MMSE).[22] The study protocol was approved by the Institutional Review Board (No. 2023–09-C031). Informed consent was obtained from all the participants.

MRI Acquisition

All MRI examinations were conducted using a 3.0T MRI scanner (Ingenia CX; Philips Healthcare, Best, Netherlands) with a 32-channel head coil. A comprehensive brain imaging protocol was conducted, including a three-dimensional (3D) turbo field echo T1-weighted scan (TFE T1WI), a T2-weighted spin echo (SE) sequence, a 3D fluid-attenuated inversion recovery (FLAIR) scan, a DTI scan, and QSM with a SE sequence. The relative scan parameters are listed in Table 1.

Table 1 MRI Scan Parameters

3D TFE T1-weighted	Scan Parameters	3D SE T2-weighted	Scan Parameters
TR	7.1 ms	TR	3200 ms
TE	3.2 ms	TE	371 ms
FA	8°	FA	90°
FOV	256 mm	FOV	256 mm
Matrix	256 × 256	Matrix	256 × 256
Isotropic voxel size	1.0 × 1.0×1.0 mm	Isotropic voxel size	1.0 × 1.0×1.0 mm
3D FLAIR T2-weighted	**Scan parameters**	**DTI**	**Scan parameters**
TR	4800 ms	TR	8424 ms
TE	338 ms	TE	78 ms
FOV	220 mm	FOV	224 mm
Matrix	324 × 324	Matrix	112 × 112
Isotropic voxel size	0.68 × 0.68×3.0 mm	Isotropic voxel size	2.0 × 2.0×2 mm
QSM	**Scan parameters**		
TR	62 ms	Matrix	384 × 314
TE	6.8 ms	Isotropic voxel size	0.6 × 0.6×2 mm
FOV	230 mm		

Abbreviations: 3D, 3-dimensional; DTI, diffusion tensor imaging; FLAIR, fluid-attenuated inversion recovery; FOV, field of view; MRI, magnetic resonance imaging; QSM, quantitative susceptibility mapping; SE, spin echo; TE, echo time; TFE, turbo field echo; TI, inversion time; TR, repetition time; TSE, turbo spin echo.

Imaging Postprocessing and Review

Two diagnostic imaging experts (> 10 years of experience) jointly reviewed the radiographs. The reviewers were blinded to the clinical diagnoses and independently performed visual analyses twice. In cases of disagreement between the two experts, a third radiologist with 30 years of experience performed visual analyses to reach a final conclusion. The main imaging analysis process was shown in Figure 1.

Visual analysis of the MRI T1WI, T2WI, and FLAIR images was performed to observe the size, morphology, and abnormal signal performance of the brain (including the cerebrum, cerebellum, and brainstem). Volumetric analysis of T1WI images was conducted to assess structural atrophy. Subcortical brain regions and ventricles were segmented automatically. Automatic segmentation on the United Imaging Platform identified 106 subregions, encompassing 22 temporal lobe, 20 frontal lobe, 12 parietal lobe, 8 occipital lobe, 8 cingulate gyrus, 2 insular, 12 subcortical GM structures, as well as cerebral WM structures, ventricles, the cerebellum, and additional structures. Volumes of the left and right caudate, putamen, globus pallidus, and thalamus were estimated.

Diffusion MRI were converted to NIFTI format using MRcroGL and were preprocessed using MRtrix tool (https://www.mrtrix.org/), Functional MRI of the Brain (FMRIB) Software Library (FSL) (https://fsl.fmrib.ox.ac.uk/fsl/fslwiki/) and the Advanced Normalization Tool (ANTs) (http://stnava.github.io/ANTs/). MRtrix tool was used for denoising and removing ring artifacts; use FSL to head dynamic eddy-current correction; ANTs was used for bias field correction, which was used to correct the uneven low-frequency intensity in MRI image data.

DTI reconstruction: the "BET" tool of FSL was used for brain extraction. Correction of B0 inhomogeneity distortion using images with opposite phase encoding DTI metrics, including fractional anisotropy (FA), mean diffusivity (MD), axial diffusivity (AD), and radial diffusivity (RD), were fitted using the "DTIFIT" tool.

Tractography: diffusion parameters at each voxel were modeled using FSL's "bedpostx" tool, followed by finer tracking with "probtrackx2" tool based on the estimated fiber orientations, utilizing 5000 streamline samples, a 0.5 mm step length, and a 0.2 curvature threshold. The 1% threshold of way total for tracking results cards is trace.nii.gz. Each case was tracked the cerebello-thalamo-motor cortical network (tremor network) and nigrostriatal-thalamo-motor cortical network (PD network).

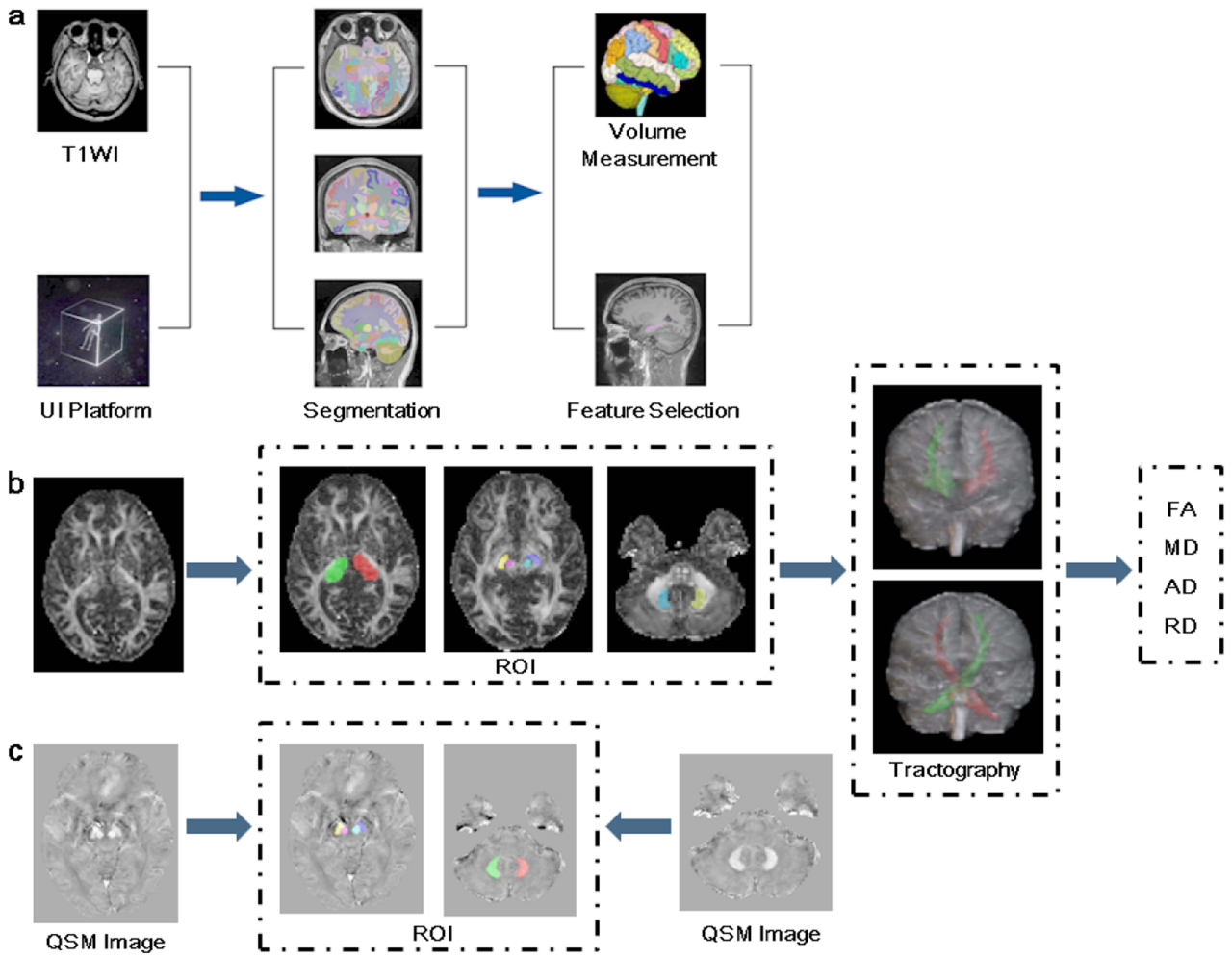

Figure 1 Workflow of the whole processing procedure. (**a**). the processing procedure of volumetric quantitative analysis of structural MRI. (**b**). DTI processing procedure, including diffusion MRI preprocess, DTI reconstruction and diffusion metrics acquisition, and tractography. (**c**). the processing procedure of quantitative analysis of QSM. **Abbreviations**: DTI, diffusion tensor imaging; MRI, magnetic resonance imaging; QSM, quantitative susceptibility mapping.

The magnitude image was scalped by the "BET" tool of FSL, magn_brain and corresponding mask were obtained, and the QSM indicator graph was calculated by STISuite. Visual analysis of QSM data in N1, situated in the dorsal region of the healthy substantia nigra (SN), at its intermediate and caudal levels. N1 appeared as an oval region with low signal intensity, encircled by a hyperintense area on QSM. N1 visual analysis employed a 3-point ordinal scale: 0 for normal (bilateral N1 presence), 1 for non-diagnostic (indecisive unilateral or bilateral N1 presence), and 2 for pathological (bilateral N1 absence). The analytical methods used were similar to those described previously.[23]

Susceptibility maps were generated by ITK-SNAP, and two experienced neurologists blinded to participant diagnoses, manually segmented Regions of Interest (ROIs). Magnetic susceptibility measurements were acquired from both brain hemispheres in the SN, red nucleus (RN), and dentate nucleus (DN) regions.

Data Analysis

Statistical analyses were performed using IBM SPSS Statistic, Version 26.0 (IBM Corporation, Armonk, NY, USA). The study compared image differences across three groups: ET, PD, and normal participant (NP). Independent samples *t*-tests evaluated differences in image parameters of the cerebello-thalamo-motor cortical network and nigrostriatal-thalamo-motor cortical network, as well as the magnetic susceptibility of SN, RN, and DN across different groups (ET vs NP, PD vs NP, and ET vs PD). All differences with a two-tailed P-value < 0.05 were deemed statistically significant.

Results

Clinical Characteristics

The pedigree of the family was obtained (Figure 2). The study included 16 of 20 family members across three generations who underwent genetic sequencing analysis and multimodal MRI, excluding the four who did not undergo MRI scans. According to the diagnostic criteria, three patients were identified with PD, and six patients were diagnosed with ET. Three patients with PD experienced tremors for multiple years prior to the onset of clinical symptoms. Case I-2 was excluded due to the patient died at the age of 75 years during the study period, while based on the available disease history provided by her grandchildren, the diagnosis of this case was consistent with "clinically possible" PD. The proband (case II-4) was a 73-year-old male who first experienced action hand tremors at 65 years of age. He then developed resting tremors in the right upper extremity, and gradually developed resting tremors in the right lower extremity and left upper extremity, along with bradykinesia, a stiff facial expression, reduced arm swing during walking, a shuffling gait, and occasional coughing while drinking water for 71 years. His past medical history included the presence of diabetes mellitus. PD was first diagnosed with a UPDRS Part III score of 45, and the patient was completely independent. He was firstly administered levodopa and benserazide hydrochloride (0.0625 g) orally three times a day; 2 weeks later, the dosage was increased to 0.125 g per dose. The patient was followed up for 1 month after medication. The patient's older sister (case II-2) had a similar disease course and treatment. Cases III-2, 4, 6, 10, 15, and IV-2 presented hand action tremors, accompanied by head tremors in cases III-4 and 15, but not in cases III-2, 6, 10, and IV-2). These tremors intensified with nervousness, subsided with alcohol consumption, and did not perform PD's manifestations. The other patients (cases II-6, 9, III-7, 19, and IV-3–6) exhibited no clinical symptoms of ET and/or PD. Table 2 provides a summary of the clinical manifestations observed in all participants.

Our previous study has reported that the proband (case II-4) was identified to have a missense mutation in the eukaryotic translation initiation factor 4 gamma 1 (*EIF4G1*) gene: c.1909A>T in exon 13; genomic coordinates, chr3:184040722. Family members II-2, 6, 9, III-2, 4, 6, 7, 10, 15, and IV-2–6 all carried the same heterozygous missense mutation in the *EIF4G1* gene: c.1909A>T. For case III-19, no mutation in this gene was identified.[24]

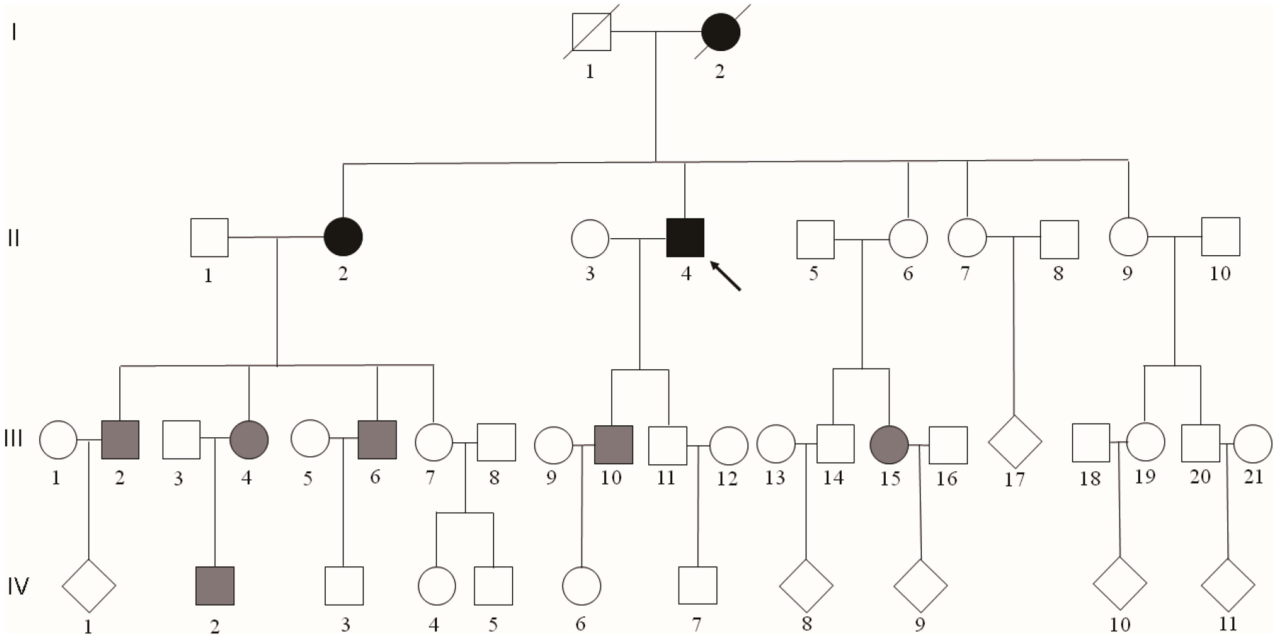

Figure 2 The pedigree of the Parkinson's disease with "antecedent essential tremor" kindred. (**I**) represents first generation; (**II**) represents second generation; (**III**) represents third generation; (**IV**) represents fourth generation. The square represents the male, the circle represents the female, and the diamond represents the gender protection, not revealing the gender; black for Parkinson's disease, grey for essential tremor; slash lines represent deceased family members; the arrows represent the proband.

https://doi.org/10.2147/NDT.S498644

Table 2 Clinicopathological Features of Individuals Within the Family

Family Member	Sex	Age at ET Onset	Age at PD Onset	Age at Examination	Disease Duration	Resting Tremor	Action Tremor	MMSE Scoring	UPDRS III Scoring	Concomitant Diseases
I-2	F	<60	70	-	>15	+	-	-	-	-
II-2	F	68	74	75	7	+	-	22	35	Hypertension
II-4	M	65	71	73	8	+	-	23	45	Diabetes
II-6	F	-	-	69	-	-	-	-	-	-
II-9	F	-	-	57	-	-	-	-	-	-
III-2	M	45	-	56	11	-	+	26	-	-
III-4	F	36	-	53	17	-	+	28	-	-
III-6	M	47	-	52	5	-	+	24	-	-
III-7	F	-	-	48	-	-	-	-	-	-
III-10	M	47	-	52	5	-	+	30	-	-
III-15	F	38	-	41	3	-	+	30	-	-
III-19	F	-	-	32	-	-	-	-	-	-
IV-2	M	20	-	27	7	-	+	30	-	-
IV-3	M	-	-	21	-	-	-	-	-	-
IV-4	F	-	-	23	-	-	-	-	-	-
IV-5	M	-	-	16	-	-	-	-	-	-
IV-6	M	-	-	14	-	-	-	-	-	-

Abbreviations: ET, essential tremor; MMSE, mini-mental state examination; PD, Parkinson's disease; UPDRS III, United Parkinson's Disease Rating Scale Part III.

MRI Manifestations

The main structural MRI manifestations of the three generations are summarized in Table 3. The proband (case II-4) and his older sister (case II-2) showed brain atrophy, periventricular WM degeneration, multiple ischemic foci, old infarct and softening foci in the bilateral brain hemispheres and basal ganglia. Case II-6 showed brain atrophy, periventricular WM degeneration, multiple ischemic foci, old infarct and softening foci in the bilateral brain hemispheres and basal ganglia. Case IV-2 showed a posterior horn cyst of the right lateral ventricle with compression and deformation of the surrounding brain tissue. No obvious abnormalities on structural MRI in other participant family members.

Compared to the NP family members, ET cases had significant lower FA in the left cerebello-thalamo-motor cortical network (P = 0.029), PD cases had significant higher AD in the left cerebello-thalamo-motor cortical network (P =

Table 3 Structural Imaging Performances of Individuals Within the Family

Family Member	Visual Analysis of Structural MRI	Volume Changes Volume (cm^3)/Volumetric Fraction (%)
I-2	-	-
II-2	Brain atrophy; Periventricular white matter degeneration; Multiple ischemic degeneration foci, old infarct foci and softening foci in the bilateral cerebral hemispheres and basal ganglia	↓ right CN (0.75/0.06), PUT (2.02/0.16), GP (1.14/0.09), TH (4.52/0.36); ↓ right side of the brain WM (168.5/13.3)
II-4	Brain atrophy; Periventricular white matter degeneration; Multiple ischemic degeneration foci, old infarct foci and softening foci in the bilateral cerebral hemispheres and basal ganglia	↓ right CN (2.32/0.16), PUT (2.78/0.19), GP (1.62/0.11), TH (5.25/0.36); ↓ right side of the brain WM (199.9/13.73); ↓ right frontal pole (0.94/0.06); ↓ left inferior parietal lobule (8.46/0.58)
II-6	Brain atrophy; Periventricular white matter degeneration; Multiple ischemic degeneration foci, old infarct foci and softening foci in the bilateral cerebral hemispheres and basal ganglia	↓ left side in the medial temporal lobe olfactory cortex (1.22/0.09)
II-9	No obvious structural abnormalities	-

(*Continued*)

Table 3 (Continued).

Family Member	Visual Analysis of Structural MRI	Volume Changes Volume (cm^3)/Volumetric Fraction (%)
III-2	No obvious structural abnormalities	↓ left GP (1.72/0.11); ↓ right superior temporal gyrus (10.11/0.66); ↓ right anterior central frontal gyrus (12.33/0.8);
III-4	No obvious structural abnormalities	↓ left medial temporal fusiform gyrus (6.91/0.53)
III-6	No obvious structural abnormalities	↓ right medial temporal fusiform gyrus (7.89/0.51), right lateral temporal lobe superior temporal gyrus (10.22/0.66); ↓ right anterior central frontal gyrus (12.13/0.79), frontal pole (0.91/0.06), left frontal triangulum (2.73/0.18); ↓ right parietal paracentral lobule (3.21/0.21); right posterior cingulate gyrus (2.71/0.18)
III-7	No obvious structural abnormalities	-
III-10	No obvious structural abnormalities	↓ right frontal pole (0.94/0.06); ↓ left frontal pole (0.79/0.05)
III-15	No obvious structural abnormalities	↓right fusiform gyrus of the medial temporal lobe (5.98/0.47)
III-19	No obvious structural abnormalities	↓ right middle temporal gyrus of later temporal lobe (8.55/0.64)
IV-2	Posterior horn cyst of right lateral ventricle with compression and deformation of surrounding brain tissue	-
IV-3	No obvious structural abnormalities	-
IV-4	No obvious structural abnormalities	-
IV-5	No obvious structural abnormalities	-
IV-6	No obvious structural abnormalities	-

Notes: ↓ Decrease of the volume (cm^3)/Volumetric fraction (%).
Abbreviations: CN, caudate nucleus; MRI, magnetic resonance imaging; PUT, putamen; GP, globus pallidus; TH, thalamus; WM, white matter.

0.0003) and MD in the right nigrostriatal-thalamo-motor cortical network ($P = 0.0012$). Compared PD family members with ET family members, no difference was detected in any other diffusion metrics (Figure 3).

The proband (case II-4) and his older sister (case II-2) showed nigrosome-1 (N1) absent bilaterally (2 score); Cases III-2, 4, 6 showed indecisive presence of N1 bilaterally (1 score); Another participant family members showed no signal abnormality in visual analysis of QSM (0 score). According to quantitative analysis of QSM, ET cases' magnetic susceptibility was significantly higher in the right SN ($P = 0.007$), the bilateral RN ($P_{L\text{-}RN} = 0.004$, $P_{R\text{-}RN} = 0.013$), and the left DN ($P = 0.007$) when compared to the NPs. PD cases' magnetic susceptibility was obvious higher in the right SN ($P = 0.015$) and the bilateral RN ($P_{L\text{-}RN} = 0.046$, $P_{R\text{-}RN} < 0.0001$) when compared to the NPs. The magnetic susceptibility was significantly different in the right RN ($P = 0.016$) between PD cases and ET cases (Figure 4). Two examples by multimodal MRI are shown in Figures 5 and 6. Multivariate analysis showed that the increased magnetic susceptibility of L-RN was the best indicator for distinguishing ET from NP, the increased magnetic susceptibility of R-RN was the best indicator for distinguishing PD from NP, and significantly different in the R-RN between PD and ET.

Discussion

This study presents clinical and multimodal MRI features of a kindred with ET and PD with "antecedent ET". Three main imaging findings were indicated as follows: 1) Quantitative analysis of structural MRI showed a reduction in the volume or volumetric fraction of frontotemporal areas to different degrees in ET and PD cases, and an additional decrease in volume or volumetric fraction of the basal ganglia nucleus in PD cases, which including the caudate nucleus (CN), putamen (PUT), globus pallidus (GP), and thalamus (TH). 2) DTI showed that the cerebello-thalamo-motor cortical network was involved in both ET and PD cases, and the additional nigrostriatal-thalamo-motor cortical network was involved in PD cases. 3) QSM revealed that N1 signals were gradually enhanced with age and disease progression (ET-to-PD transition), and PD cases' magnetic susceptibility was significantly higher in RN compared with ET cases, and in

https://doi.org/10.2147/NDT.S498644

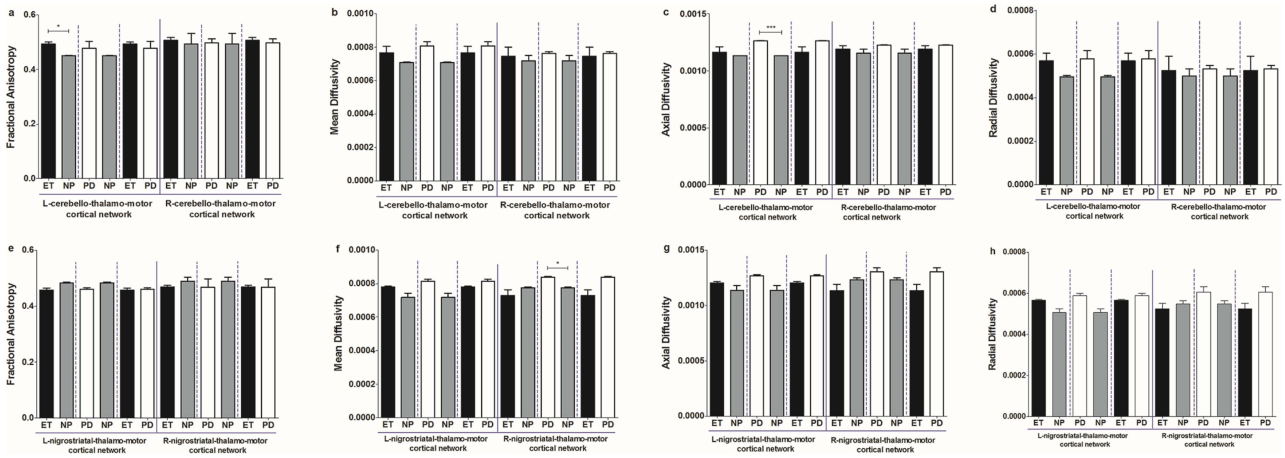

Figure 3 Intergroup differences in diffusion metrics of the cerebello-thalamo-motor cortical network and nigrostriatal-thalamo-motor cortical network. (**a**. and **e**.) statistics differences in fractional anisotropy of cerebello-thalamo-motor cortical network and nigrostriatal-thalamo-motor cortical network in ET vs NP, PD vs NP and ET vs PD. (**b**. and **f**). statistics differences in mean diffusivity of cerebello-thalamo-motor cortical network and nigrostriatal-thalamo-motor cortical network in ET vs NP, PD vs NP and ET vs PD. (**c**. and **g**). statistics differences in axial diffusivity of cerebello-thalamo-motor cortical network and nigrostriatal-thalamo-motor cortical network in ET vs NP, PD vs NP and ET vs PD. (**d**. and **h**). statistics differences in radial diffusivity of cerebello-thalamo-motor cortical network and nigrostriatal-thalamo-motor cortical network in ET vs NP, PD vs NP and ET vs PD. *$P < 0.05$.

Abbreviations: ET, essential tremor; NP, normal participant; PD, Parkinson's disease.

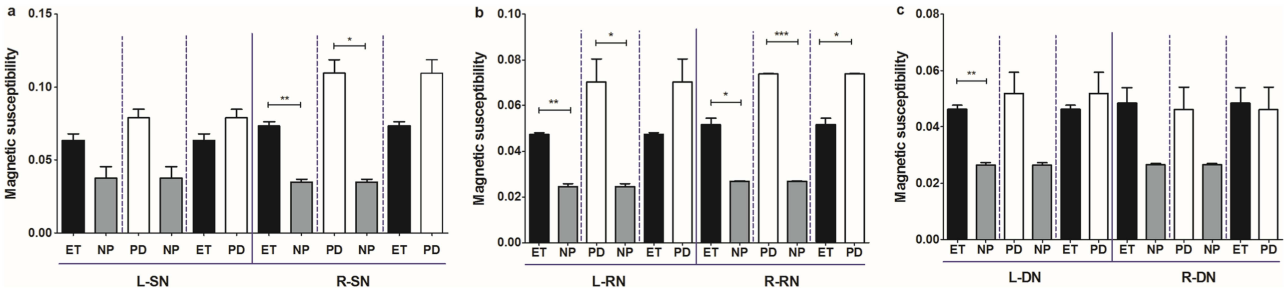

Figure 4 Intergroup differences in magnetic susceptibility in the SN, RN, and DN. (**a**). statistics differences in magnetic susceptibility of SN in ET vs NP, PD vs NP and ET vs PD. (**b**). statistics differences in magnetic susceptibility of RN in ET vs NP, PD vs NP and ET vs PD. (**c**). statistics differences in magnetic susceptibility of DN in ET vs NP, PD vs NP and ET vs PD. *P < 0.05; **P < 0.01; ***P < 0.001.

Abbreviations: DN, dentate nucleus; ET, essential tremor; NP, normal participant; PD, Parkinson's disease; RN, red nucleus; SN, substantia nigra.

addition to the high magnetic susceptibility in SN and RN, ET cases showed an additional high magnetic susceptibility in DN.

ET and PD are common but distinct neurological diseases with overlapping features. These two diseases tend to co-occur in a kindred. Previous studies have found that patients with ET are four fold higher risk to develop PD compared to those without ET.[25] To date, there are no adequate biomarkers for early differential diagnosis or precise prediction of the progression of these two diseases.

Current clinical diagnoses of ET and PD primarily rely on evaluating phenomenological traits and the disease progression. Our findings indicate that the application of noninvasive multimodal imaging can enhance the objectivity of differential diagnosis of ET and PD based on clinical diagnoses. While no specific neuroimaging method is advised for routine clinical use in ET and PD, various previous studies have noted imaging differences between the two diseases, though many findings remained controversial. For ET cases, cerebellar and cerebral structural changes are distinctly heterogeneous and are associated with clinical phenotypes.[26] A number of neuroimaging studies have reported cerebellar or cerebral atrophy (especially in the cerebellar deep nucleus and in the cerebral cortex or subcortical gyrus),[27,28] no morphological cerebellar changes,[29,30] or even increased cerebellar and cerebral GM volume in patients with ET compared to normal controls.[31,32] In our study, no morphological cerebellar changes were observed in the kindred with ET, mainly manifesting as a reduction in frontotemporal cortical volume, and only one patient had additional GP

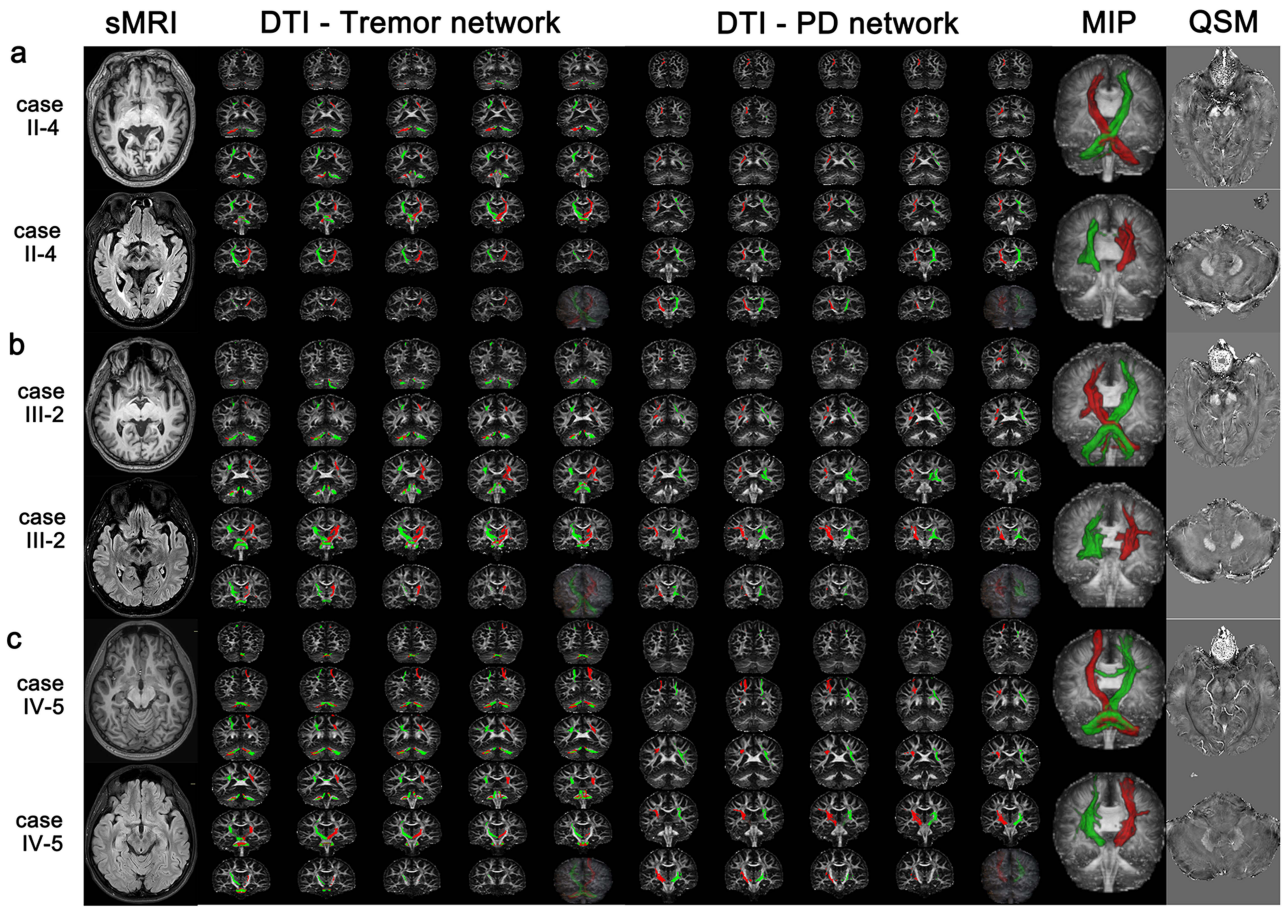

Figure 5 Multimodal imaging performed in the three generations. First column: sMRI; second column: DTI-Tremor network; third column: DTI-PD network; fourth column: DTI-MIP; and fifth column: QSM. (**a**). the multimodal MRI findings of the proband (case II-4). (**b**). the multimodal MRI findings of the case III-2. (**c**). the multimodal MRI findings of the case IV-5.

Abbreviations: DTI, diffusion tensor imaging; MIP, maximum intensity projection; PD, Parkinson's disease; QSM, quantitative susceptibility mapping; sMRI, structural magnetic resonance imaging.

atrophy. We suggest that a reduction in the GM volume of the basal ganglia nucleus may be a significant indicator of ET progression. Structural changes on conventional MRI in patients with PD are less apparent, especially in the early stage. Previous neuroimaging studies have documented brainstem and subcortical involvement in PD's early stages, and atrophy in different brain regions as the disease progresses.[33,34] A voxel-based morphometry analysis of PD found that basal ganglia atrophy aligned with nigrostriatal degeneration, and lead to the dysfunction of the basal ganglia thalamo-cortical circuit;[35] frontotemporal and occipitoparietal cortical regions were also involved in the advanced stage. The results of our structural MRI visual analysis and quantitative volume analyses yielded results consistent with previous studies. We found that morphological changes in the basal ganglia may be potential markers of ET transformation into PD, which aligned with its pathophysiological function of motor regulation.

The application of DTI in ET and PD has been extensively studied. MRI studies have demonstrated DTI techniques could provide evidence for regional altered WM microstructural integrity in ET and PD. How to use DTI to distinguish ET and PD has important clinical application value. Previous studies mostly analyzed the DTI data of certain fiber bundle segments. In patients with ET, FA values in the DN and cerebral multi-region WM fiber tracts were decreased compared with healthy controls.[16,36] When compared to PD patients, ET patients exhibited more pronounced involvement of the DN, cerebellar peduncles, and thalamo-cortical visual pathway, with no observed differences in the SN.[16] While another study reported that the AUC was 0.96 using DTI measures from the CN and SN to differentiate PD from ET.[37] Currently, both ET and PD are considered network diseases of brain. The cerebello-thalamo-cortical network, as one of tremor-related pathways, has been indicated to be the mostly involved in ET pathophysiological processes.[38] The present study

https://doi.org/10.2147/NDT.S498644

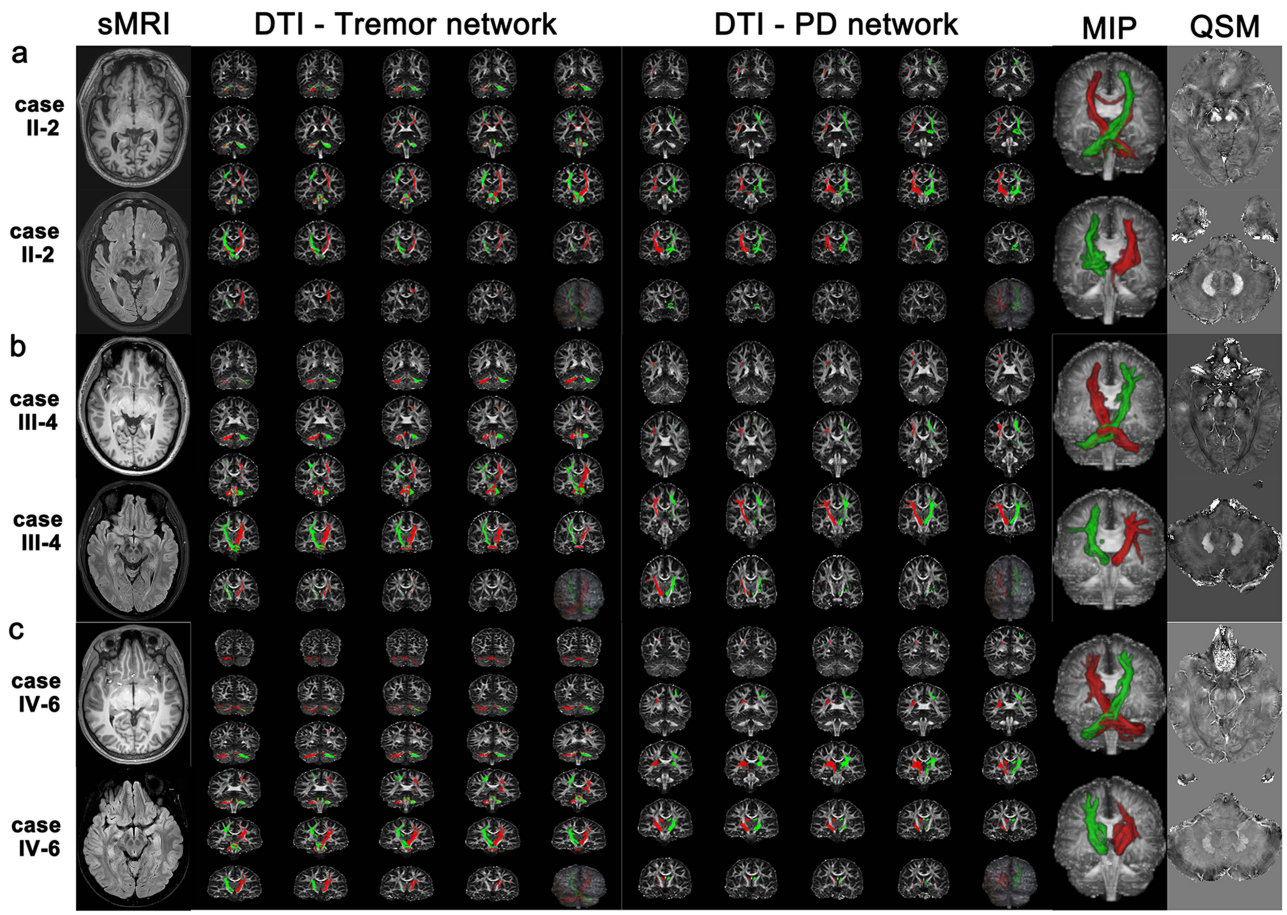

Figure 6 Multimodal imaging performed in the three generations. First column: sMRI; second column: DTI-Tremor network; third column: DTI-PD network; fourth column: DTI-MIP; and fifth column: QSM. (**a**). the multimodal MRI findings of the case II-2. (**b**). the multimodal MRI findings of the case III-4. (**c**). the multimodal MRI findings of the case IV-6.

Abbreviations: DTI, diffusion tensor imaging; MIP, maximum intensity projection; PD, Parkinson's disease; QSM, quantitative susceptibility mapping; sMRI, structural magnetic resonance imaging.

analyzed the DTI data of the involved network, and confirmed the changes of WM microstructure in cerebello-thalamo-cortical network in ET cases.[39] In addition, our results showed an increased structural connection in cerebello-thalamo-cortical pathway of PD compared to NP, which may be potentially attributable to the early stages and tremor-dominant nature of PD. The spatial position relationship of cerebello-thalamo-cortical network in these two diseases persists greatly overlap. In PD, studies have confirmed that lower structural connectivity in the motor network encompassing striatum, GP, TH and motor cortex corresponds to the pathophysiology of PD.[40] We analyzed the nigrostriatal-thalamo-motor cortical network in each case within this kindred, and found that PD cases showed dysfunction of this network. The dysfunction of the nigrostriatal-thalamo-motor cortical network could serve as a potential neuroimaging marker for predicting disease progression, and may be linked to brain iron deposition in PD cases.

Key pathological changes in PD include the progressive degeneration of dopaminergic neurons and iron accumulation in the SN.[41] QSM has been used in several studies to quantify iron content, and it is sensitive in detecting iron-correlated changes in the brains of PD patients.[42] QSM is a promising diagnostic tool for PD.[43] Fu et al confirmed that dynamic measurement of iron deposition by QSM in the subcortical nuclei (SN, RN, CN, GP, and PUT) can be used to monitor disease progression.[18] An MRI study indicated that ET was also linked to iron deposition in the SN; however, the degree of iron deposition was significantly lower than that in PD patients.[23] We initially conducted a visual analysis of N1 due to its rapid and convenient nature for clinical use. Our study showed that visual analysis has a fairly strong diagnostic capability for PD, while variations in its effectiveness for ET (with or without iron deposition in nigra striatum). Quantitative analysis of QSM revealed significantly elevated iron concentration in the DN of ET cases compared to NPs,

and in the RN of PD cases compared to ET cases. Previous studies have indicated a correlation between excessive iron deposition in DN and tremor,[16,44] and Duanmu et al indicated DN iron deposition in action tremor,[45] which was consistent with our result. The RN is an essential part of the cerebello-thalamo-cortical network, and abnormalities in the RN can cause the dysfunction of this circuit, resulting in tremors. However, the specific role of iron deposition in the RN for pathogenesis of ET remains unclear, and most studies have indicated that no obvious signs of iron deposition were found in the RN in ET patients. Abnormal iron deposition in the RN and other regions is a prominent feature of PD, and heightened iron accumulation in the RN is related to PD progression.[46,47] Previous studies have suggested that the iron deposition in the RN can be used as a reference for the differential diagnosis of ET and PD. However, our results were slightly different from previous studies. Our study showed iron deposition was found in the RN of ET cases, while more obvious iron accumulation in the RN of PD cases. Combining visual and quantitative analysis, we propose that gradually increasing iron deposition in the SN and RN could serve as a diagnostic biomarker for distinguishing PD from ET and as a predictor of ET progression to PD, and iron deposition in the DN may serve as an effective tool for ET severity stratification.

The present study is limited, and the data is relatively very scanty. The main reason is a relatively small sample size and the short longitudinal follow-up time. Regular follow-up of all family members with MRI and inclusion of more families are needed to meet the requirements of future longitudinal studies.

Conclusions

Our study found that morphological changes in the basal ganglia, microstructural dysfunction in the nigrostriatal-thalamo -motor cortical network and iron deposition could as potential imaging biomarkers for diagnosing ET and PD and could be an effective tool for the longitudinal monitoring of disease progression and transformation. The heterogeneous temporal-spatial features of morphology and iron deposition across various brain regions highlighted the importance of monitoring dynamic changes in iron content, WM microstructure and morphology throughout the progression of this kindred. These approaches enhance our understanding iron metabolism dynamics and structural connection network changes in the pathogenesis of PD with “antecedent ET”, aiding in the development of novel methods for predicting disease progression.

Abbreviations

3D TFE T1WI, three-dimensional turbo field echo T1-weighted scan; AD, axial diffusivity; ANTs, Advanced Normalization Tool; CN, caudate nucleus; DN, dentate nucleus; DTI, Diffusion tensor imaging; *EIF4G1*, eukaryotic translation initiation factor 4 gamma 1; ET, essential tremor; FA, fractional anisotropy; FLAIR, fluid-attenuated inversion recovery; FMRIB, functional magnetic resonance imaging of the brain; FSL, FMRIB software library; GP, globus pallidus; MD, mean diffusivity; MRI, magnetic resonance imaging; N1, nigrosome-1; NP, normal participant; PD, Parkinson’s disease; PUT, putamen; QSM, quantitative susceptibility mapping; RN, red nucleus; ROIs, Regions of Interest; SE, spin echo; SN, substantia nigra; T2WI, T2-weighted; TH, thalamus; WM, white matter.

Data Sharing Statement

The datasets generated and analyzed in this study are available in the ClinVar (accession no. SCV004039569; https://www.ncbi.nlm.nih.gov/clinvar). Other datasets used and/or analyzed in this study are available from the corresponding author on reasonable request.

Consent to Participate

Informed consent was obtained from all individual participants included in the study.

Consent to Publish

All the participants provided informed consent to publish.

Ethics Approval

The study was performed in line with the principles of the Declaration of Helsinki. Approval was granted by the Medical Ethics Committee of the Affiliated Hospital of Jining Medical University (No. 2023-09-C031).

Acknowledgments

We would like to extend our deepest appreciation to the clinical physicians and technicians at the Department of Neurology of the Affiliated Hospital of Jining Medical University.

An unauthorized version of the Chinese MMSE was used by the study team without permission, however this has now been rectified with PAR. The MMSE is a copyrighted instrument and may not be used or reproduced in whole or in part, in any form or language, or by any means without written permission of PAR (www.parinc.com).

Funding

This work was supported by Shandong Provincial Natural Science Foundation [ZR2023QH076]; the Youth Innovation Technology Project of Higher School in Shandong Province [2023KJ261]; the Key Research and Development Plan of Jining City [2023YXNS158, 2023YXNS227]; Research Fund for Lin He's Academician Workstation of New Medicine and Clinical Translation in Jining Medical University [JYHL2021FMS18, JYHL2022FMS05]; and the postdoctoral program of the Affiliated Hospital of Jining Medical University [JYFY322153].

Disclosure

The authors have no relevant financial or non-financial interests to disclose in this work.

References

1. Bhatia KP, Bain P, Bajaj N, et al. Consensus Statement on the classification of tremors. from the task force on tremor of the International Parkinson and Movement Disorder Society. *Movement disorders*. 2018;33(1):75–87. doi:10.1002/mds.27121
2. Lees AJ, Hardy J, Revesz T. Parkinson's disease. *Lancet*. 2009;373(9680):2055–2066. doi:10.1016/s0140-6736(09)60492-x
3. Hajek A, Grupp K, Aarabi G, Kretzler B, König HH. Parkinson's disease and subjective prospects for the future in different life domains. findings of a nationally representative sample. *Neuropsychiatr Dis Treat*. 2023;19:1791–1798. doi:10.2147/NDT.S412366
4. Zhang T, Yang R, Pan J, Huang S. Parkinson's disease related depression and anxiety: a 22-year bibliometric analysis (2000-2022). *Neuropsychiatr Dis Treat*. 2023;19:1477–1489. doi:10.2147/NDT.S403002
5. Tarakad A, Jankovic J. Essential tremor and Parkinson's disease: exploring the relationship. *Tremor Other Hyperkinet Mov*. 2018;8:589. doi:10.7916/d8md0gvr
6. Heim B, Peball M, Krismer F, Djamshidian A, Seppi K. Pimavanserin: a truly effective treatment for Parkinson's disease psychosis? A review of interventions. *Neuropsychiatr Dis Treat*. 2023;19:1303–1312. doi:10.2147/NDT.S371641
7. Saeed U, Lang AE, Masellis M. Neuroimaging advances in Parkinson's disease and atypical parkinsonian syndromes. *Front Neurol*. 2020;11:572976. doi:10.3389/fneur.2020.572976
8. Postuma RB, Berg D, Stern M, et al. MDS clinical diagnostic criteria for Parkinson's disease. *Mov Disord*. 2015;30(12):1591–1601. doi:10.1002/mds.26424
9. Sarica A, Quattrone A, Crasà M, et al. Cerebellar voxel-based morphometry in essential tremor. *J Neurol*. 2022;269(11):6029–6035. doi:10.1007/s00415-022-11291-9
10. Sharifi S, Nederveen AJ, Booij J, van Rootselaar AF. Neuroimaging essentials in essential tremor: a systematic review. *Neuroimage Clin*. 2014;5:217–231. doi:10.1016/j.nicl.2014.05.003
11. Yadav SK, Rai SN, Singh SP. Mucuna pruriens reduces inducible nitric oxide synthase expression in Parkinsonian mice model. *J Chem Neuroanat*. 2017;80:1–10. doi:10.1016/j.jchemneu.2016.11.009
12. Rai SN, Yadav SK, Singh D, Singh SP. Ursolic acid attenuates oxidative stress in nigrostriatal tissue and improves neurobehavioral activity in MPTP-induced Parkinsonian mouse model. *J Chem Neuroanat*. 2016;71:41–49. doi:10.1016/j.jchemneu.2015.12.002
13. Prakash J, Chouhan S, Yadav SK, Westfall S, Rai SN, Singh SP. Withania somnifera alleviates parkinsonian phenotypes by inhibiting apoptotic pathways in dopaminergic neurons. *Neurochem Res*. 2014;39(12):2527–2536. doi:10.1007/s11064-014-1443-7
14. Ramakrishna K, Nalla LV, Naresh D, et al. WNT-β catenin signaling as a potential therapeutic target for neurodegenerative diseases: current status and future perspective. *Diseases*. 2023;11(3). doi:10.3390/diseases11030089
15. Rai SN, Singh P. Advancement in the modelling and therapeutics of Parkinson's disease. *J Chem Neuroanat*. 2020;104:101752. doi:10.1016/j.jchemneu.2020.101752
16. Juttukonda MR, Franco G, Englot DJ, et al. White matter differences between essential tremor and Parkinson disease. *Neurology*. 2019;92(1):e30–e39. doi:10.1212/wnl.0000000000006694
17. Guan X, Lancione M, Ayton S, Dusek P, Langkammer C, Zhang M. Neuroimaging of Parkinson's disease by quantitative susceptibility mapping. *Neuroimage*. 2024;289:120547. doi:10.1016/j.neuroimage.2024.120547
18. Fu X, Deng W, Cui X, et al. Time-specific pattern of iron deposition in different regions in Parkinson's disease measured by quantitative susceptibility mapping. *Front Neurol*. 2021;12:631210. doi:10.3389/fneur.2021.631210

19. Chen Q, Boeve BF, Forghanian-Arani A, et al. MRI quantitative susceptibility mapping of the substantia nigra as an early biomarker for Lewy body disease. *J Neuroimaging*. 2021;31(5):1020–1027. doi:10.1111/jon.12878
20. Tan S, Hartono S, Welton T, et al. Utility of quantitative susceptibility mapping and diffusion kurtosis imaging in the diagnosis of early Parkinson's disease. *Neuroimage Clin*. 2021;32:102831. doi:10.1016/j.nicl.2021.102831
21. Zhang Y, Huang P, Wang X, et al. Visualizing the deep cerebellar nuclei using quantitative susceptibility mapping: an application in healthy controls, Parkinson's disease patients and essential tremor patients. *Hum Brain Mapp*. 2023;44(4):1810–1824. doi:10.1002/hbm.26178
22. Li H, Jia J, Yang Z. Mini-mental state examination in elderly Chinese: a population-based normative study. *J Alzheimers Dis*. 2016;53(2):487–496. doi:10.3233/JAD-160119
23. Jin L, Wang J, Wang C, et al. Combined visualization of nigrosome-1 and neuromelanin in the substantia nigra using 3T MRI for the differential diagnosis of essential tremor and de novo Parkinson's disease. *Front Neurol*. 2019;10:100. doi:10.3389/fneur.2019.00100
24. Liu RH, Xiao XY, Yao L, et al. Eukaryotic translation initiation factor EIF4G1 p.Ser637Cys mutation in a family with Parkinson's disease with antecedent essential tremor. *Exp Ther Med*. 2024;27(5):206. doi:10.3892/etm.2024.12494
25. Benito-León J, Louis ED, Bermejo-Pareja F. Risk of incident Parkinson's disease and parkinsonism in essential tremor: a population based study. *J Neurol Neurosurg Psychiatry*. 2009;80(4):423–425. doi:10.1136/jnnp.2008.147223
26. Lopez AM, Trujillo P, Hernandez AB, et al. Structural correlates of the sensorimotor cerebellum in Parkinson's disease and essential tremor. *Mov Disord*. 2020;35(7):1181–1188. doi:10.1002/mds.28044
27. Dyke JP, Cameron E, Hernandez N, Dydak U, Louis ED. Gray matter density loss in essential tremor: a lobule by lobule analysis of the cerebellum. *Cerebellum Ataxias*. 2017;4:10. doi:10.1186/s40673-017-0069-3
28. Prasad S, Pandey U, Saini J, Ingalhalikar M, Pal PK. Atrophy of cerebellar peduncles in essential tremor: a machine learning-based volumetric analysis. *Eur Radiol*. 2019;29(12):7037–7046. doi:10.1007/s00330-019-06269-7
29. Pietracupa S, Bologna M, Bharti K, et al. White matter rather than gray matter damage characterizes essential tremor. *Eur Radiol*. 2019;29(12):6634–6642. doi:10.1007/s00330-019-06267-9
30. Nicoletti V, Cecchi P, Frosini D, et al. Morphometric and functional MRI changes in essential tremor with and without resting tremor. *J Neurol*. 2015;262(3):719–728. doi:10.1007/s00415-014-7626-y
31. Qi S, Cao H, Wang R, Jian Z, Bian Y, Yang J. Relative increase in cerebellar gray matter in young onset essential tremor: evidence from voxel-based morphometry analysis. *J Clin Neurosci*. 2020;79:251–256. doi:10.1016/j.jocn.2020.07.003
32. Cameron E, Dyke JP, Hernandez N, Louis ED, Dydak U. Cerebral gray matter volume losses in essential tremor: a case-control study using high resolution tissue probability maps. *Parkinsonism Relat Disord*. 2018;51:85–90. doi:10.1016/j.parkreldis.2018.03.008
33. Tessitore A, Amboni M, Cirillo G, et al. Regional gray matter atrophy in patients with Parkinson disease and freezing of gait. *AJNR Am J Neuroradiol*. 2012;33(9):1804–1809. doi:10.3174/ajnr.A3066
34. Lee SY, Chen MH, Chiang PL, et al. Reduced gray matter volume and respiratory dysfunction in Parkinson's disease: a voxel-based morphometry study. *BMC Neurol*. 2018;18(1):73. doi:10.1186/s12883-018-1074-8
35. Xu X, Han Q, Lin J, Wang L, Wu F, Shang H. Grey matter abnormalities in Parkinson's disease: a voxel-wise meta-analysis. *Eur J Neurol*. 2020;27(4):653–659. doi:10.1111/ene.14132
36. Nicoletti G, Manners D, Novellino F, et al. Diffusion tensor MRI changes in cerebellar structures of patients with familial essential tremor. *Neurology*. 2010;74(12):988–994. doi:10.1212/WNL.0b013e3181d5a460
37. Prodoehl J, Li H, Planetta PJ, et al. Diffusion tensor imaging of Parkinson's disease, atypical parkinsonism, and essential tremor. *Mov Disord*. 2013;28(13):1816–1822. doi:10.1002/mds.25491
38. Helmich RC, Toni I, Deuschl G, Bloem BR. The pathophysiology of essential tremor and Parkinson's tremor. *Curr Neurol Neurosci Rep*. 2013;13(9):378. doi:10.1007/s11910-013-0378-8
39. Pietracupa S, Bologna M, Tommasin S, Berardelli A, Pantano P. The contribution of neuroimaging to the understanding of essential tremor pathophysiology: a systematic review. *Cerebellum*. 2022;21(6):1029–1051. doi:10.1007/s12311-021-01335-7
40. Filip P, Burdová K, Valenta Z, et al. Tremor associated with similar structural networks in Parkinson's disease and essential tremor. *Parkinsonism Relat Disord*. 2022;95:28–34. doi:10.1016/j.parkreldis.2021.12.014
41. Cheng Z, He N, Huang P, et al. Imaging the Nigrosome 1 in the substantia nigra using susceptibility weighted imaging and quantitative susceptibility mapping: an application to Parkinson's disease. *Neuroimage Clin*. 2020;25:102103. doi:10.1016/j.nicl.2019.102103
42. Azuma M, Hirai T, Yamada K, et al. Lateral asymmetry and spatial difference of iron deposition in the substantia nigra of patients with Parkinson disease measured with quantitative susceptibility mapping. *AJNR Am J Neuroradiol*. 2016;37(5):782–788. doi:10.3174/ajnr.A4645
43. Kang JJ, Chen Y, Xu GD, et al. Combining quantitative susceptibility mapping to radiomics in diagnosing Parkinson's disease and assessing cognitive impairment. *Eur Radiol*. 2022;32(10):6992–7003. doi:10.1007/s00330-022-08790-8
44. Welton T, Cardoso F, Carr JA, et al. Essential tremor. *Nat Rev Dis Primers*. 2021;7(1):83. doi:10.1038/s41572-021-00314-w
45. Duanmu X, Wen J, Tan S, et al. Aberrant dentato-rubro-thalamic pathway in action tremor but not rest tremor: a multi-modality magnetic resonance imaging study. *CNS Neurosci Ther*. 2023;29(12):4160–4171. doi:10.1111/cns.14339
46. Yang L, Cheng Y, Sun Y, et al. Combined application of quantitative susceptibility mapping and diffusion kurtosis imaging techniques to investigate the effect of iron deposition on microstructural changes in the brain in Parkinson's disease. *Front Aging Neurosci*. 2022;14:792778. doi:10.3389/fnagi.2022.792778
47. Li KR, Avecillas-Chasin J, Nguyen TD, Gillen KM, Dimov A. Quantitative evaluation of brain iron accumulation in different stages of Parkinson's disease. *J Neuroimag*. 2022;32(2):363–371. doi:10.1111/jon.12957